iScience, Volume *25*

Supplemental information

Structural basis for binding diversity of acetyltransferase p300 to the nucleosome

Suguru Hatazawa, Jiuyang Liu, Yoshimasa Takizawa, Mohamad Zandian, Lumi Negishi, Tatiana G. Kutateladze, and Hitoshi Kurumizaka

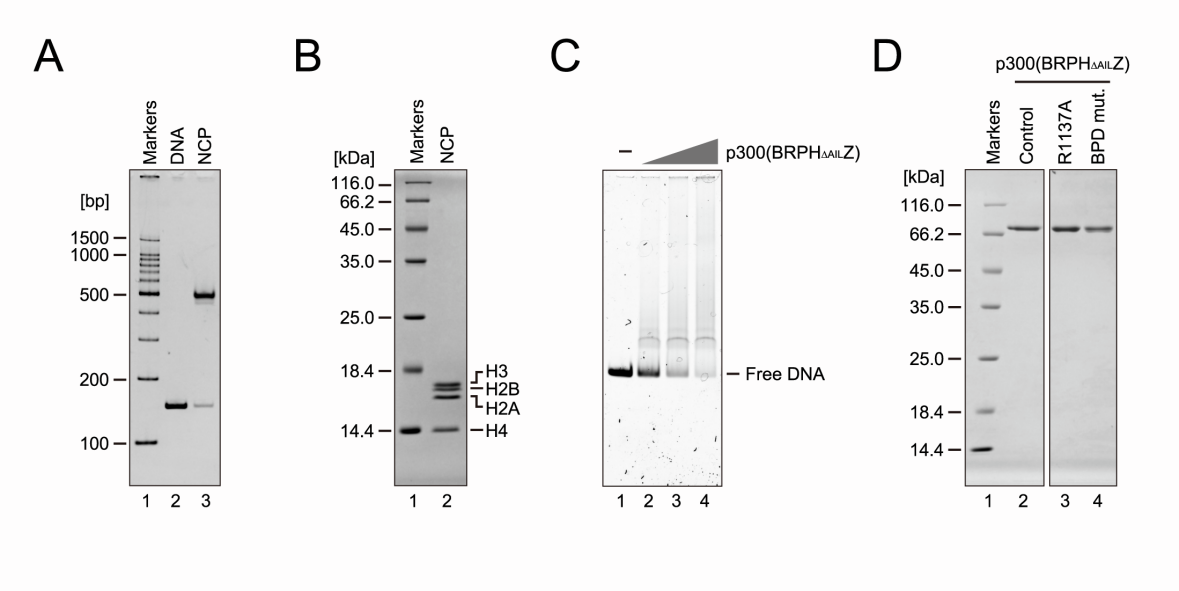

Figure S1. Preparation of the NCP and the p300(BRPH$_{\Delta AIL}$Z) proteins and assay for p300(BRPH$_{\Delta AIL}$Z)-DNA binding, related to Figures 1 and 3. (A) The 145 base-pair Widom 601 DNA and the purified NCP containing the DNA were analyzed by non-denaturing 6% polyacrylamide gel electrophoresis with ethidium bromide staining. (B) The nucleosomal histones were analyzed by 18% SDS-polyacrylamide gel electrophoresis with Coomassie Brilliant Blue staining. (C) Electrophoretic mobility shift assay of p300(BRPH$_{\Delta AIL}$Z) and the naked 145 base-pair Widom 601 DNA. The binding of p300(BRPH$_{\Delta AIL}$Z) and DNA was analyzed by non-denaturing 4% polyacrylamide gel electrophoresis with SYBR Gold staining. (D) The purified p300(BRPH$_{\Delta AIL}$Z) proteins were analyzed by 12% SDS-polyacrylamide gel electrophoresis with Coomassie Brilliant Blue staining.

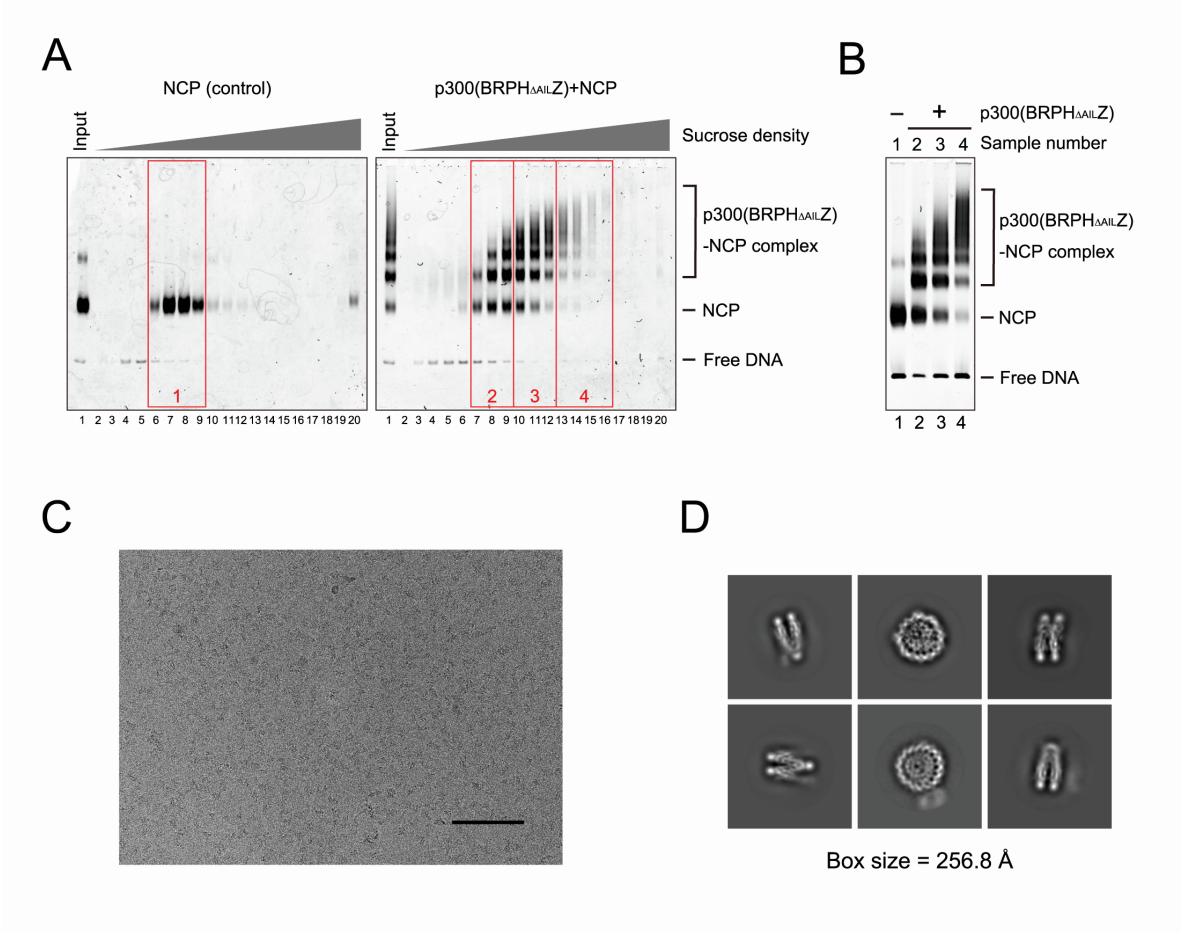

Figure S2. Preparation and cryo-EM analysis of the p300(BRPH$_{\Delta AIL}$Z)-NCP complexes, related to Figures 2 and 4. (A) The p300(BRPH$_{\Delta AIL}$Z)-NCP complexes were purified by sucrose density gradient centrifugation, and the collected fractions were analyzed by non-denaturing 4% polyacrylamide gel electrophoresis with SYBR Gold staining. The fractions shown in the red frames were combined. (B) The purified NCP and p300(BRPH$_{\Delta AIL}$Z)-NCP samples were analyzed by non-denaturing 4% polyacrylamide gel electrophoresis with SYBR Gold staining. Sample number 3 was used for the cryo-EM analysis. (C) A representative image from a digital cryo-EM micrograph of the p300(BRPH$_{\Delta AIL}$Z)-NCP complexes. Scale bar indicates 100 nm. (D) Representative 2D class averages of the p300(BRPH$_{\Delta AIL}$Z)-NCP complex from single particle images.

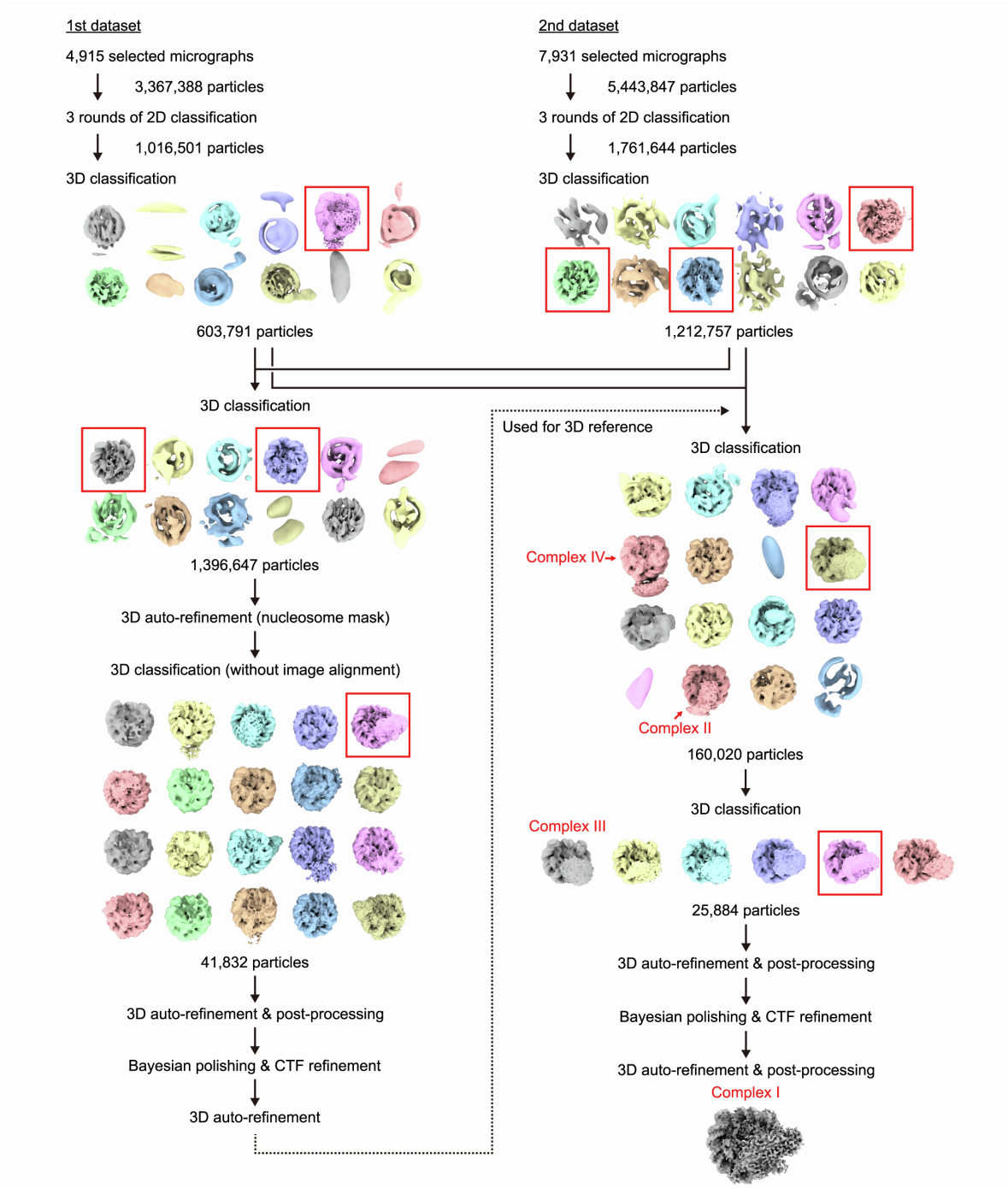

Figure S3. Workflow for cryo-EM processing of the p300(BRPH$_{\Delta AIL}$Z)-NCP complex related to Figures 2 and 4. The particles contained in the classes enclosed by the red squares were used in the subsequent processes.

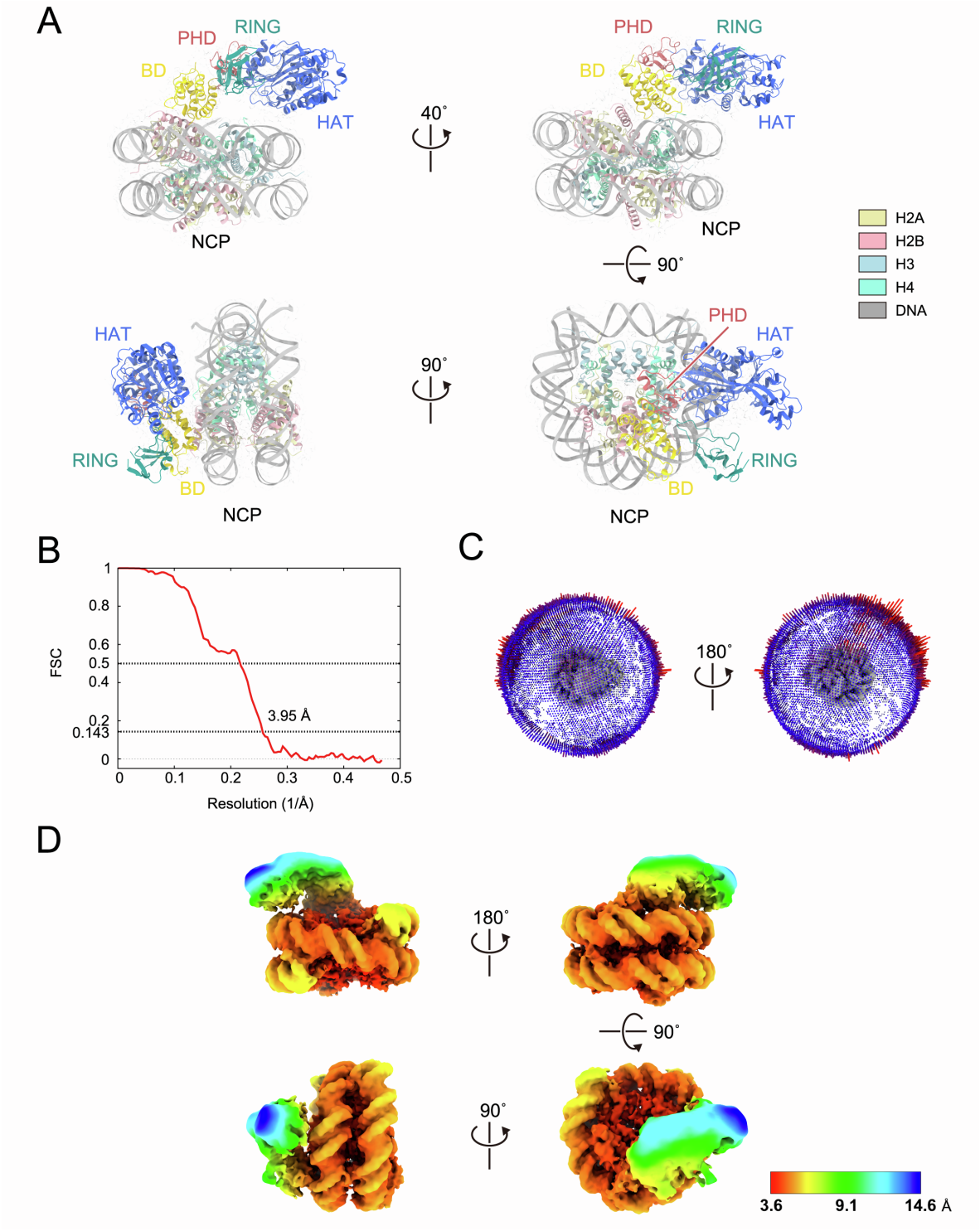

Figure S4. Cryo-EM structure of the p300(BRPH$_{\Delta AIL}$Z)-NCP complex I, related to Figure 2. (A) The overall structure of the p300(BRPH$_{\Delta AIL}$Z)-NCP complex I. The crystal structures of the NCP and

the p300 catalytic core are superimposed on the cryo-EM map. (B) Gold-standard Fourier Shell Correlation (FSC) curve of the p300(BRPH$_{\Delta AIL}$Z)-NCP complex I. Its overall resolution is 3.95 Å at FSC = 0.143. (C) Angular distribution of model projections of the p300(BRPH$_{\Delta AIL}$Z)-NCP complex I. (D) Local resolution map of the p300(BRPH$_{\Delta AIL}$Z)-NCP complex I estimated by the RELION 3.1 postprocess, showing the resolution range across the map from 3.6 Å to 14.6 Å.

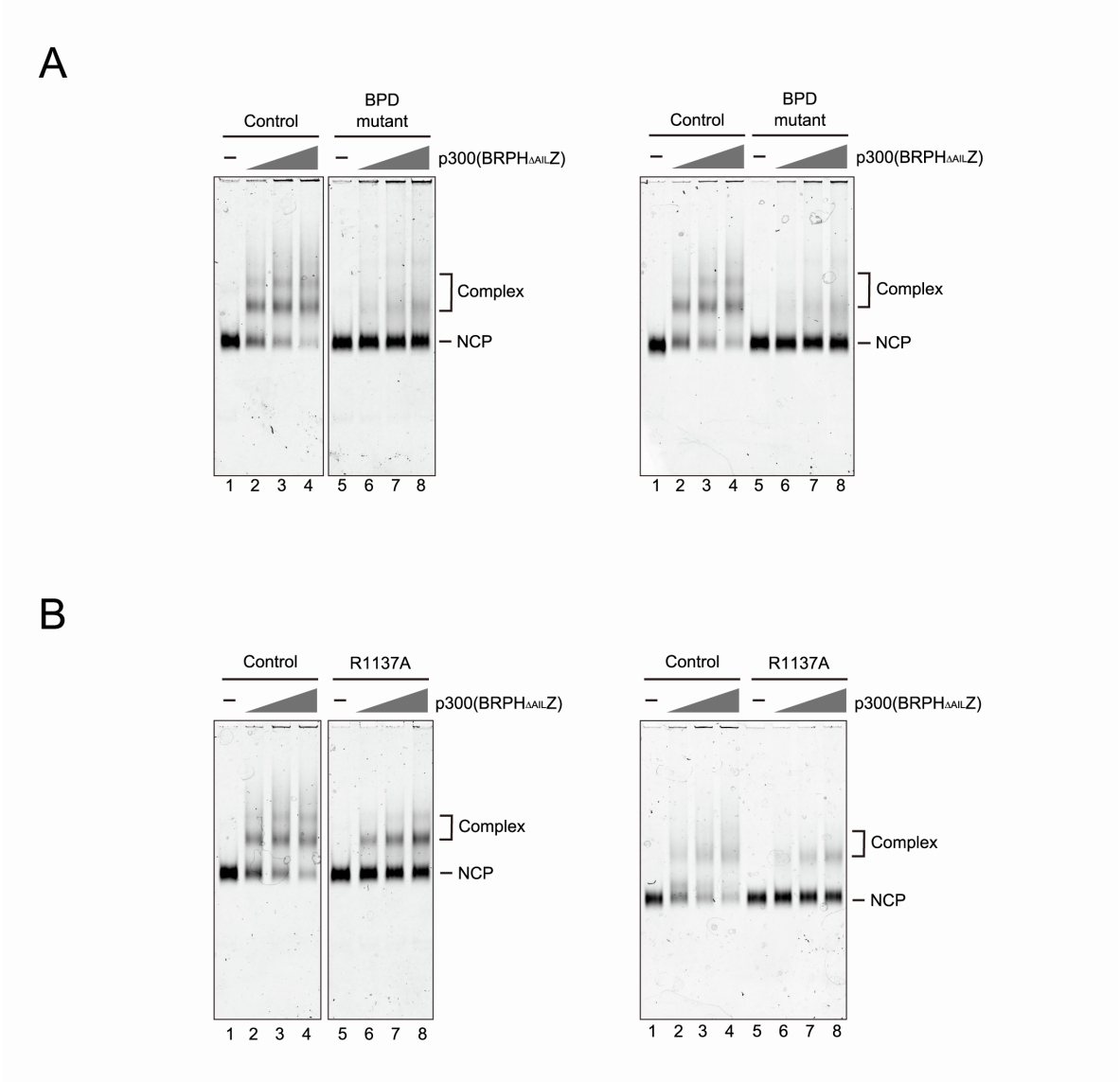

Figure S5. Replicated experiments related to Figure 3. (A) Electrophoretic mobility shift assay of the p300(BRPH$_{\Delta AIL}$Z) or p300(BRPH$_{\Delta AIL}$Z) BPD mutant (K1456A/K1459A/K1461A/R1462A) and the NCP. Complex formation was analyzed by non-denaturing 4% polyacrylamide gel electrophoresis with SYBR Gold staining. (B) Electrophoretic mobility shift assay of the p300(BRPH$_{\Delta AIL}$Z) or p300(BRPH$_{\Delta AIL}$Z) R1137A mutant and the NCP. Complex formation was analyzed by non-denaturing 4% polyacrylamide gel electrophoresis with SYBR Gold staining.